ASEAN Engineering Journal

Full Paper

PREPARATION AND RHEOLOGICAL CHARACTERIZATION OF CELLULOSE-CHITOSAN HYDROGEL FOR EXTRUSION 3D PRINTER

Gerardo Martin Quindoza III, Patrick Aldwin Castillo, Jill Manapat, John Kenneth Cruz*

Department of Mining, Metallurgical, and Materials Engineering, College of Engineering, University of the Philippines Diliman, Quezon City, Philippines

Article history
Received
5 August 2021
Received in revised form
28 November 2021
Accepted
20 January 2022
Published online
30 November 2022

*Corresponding author
jacruz1@up.edu.ph

Graphical abstract

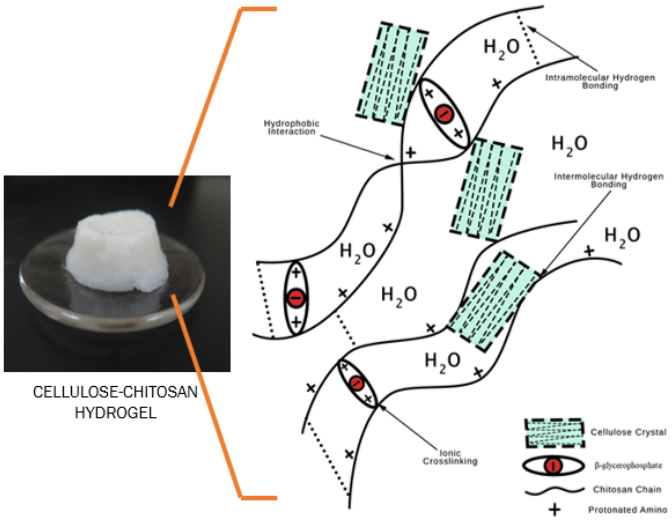

Abstract

The application of three-dimensional (3D) printing in tissue engineering is becoming prominent nowadays. A big obstacle for this technology is the selection of proper ink material. Chitosan hydrogel is an established biocompatible material that can be used as tissue scaffolds, and it has the rheology necessary for processing via extrusion type 3D printer. However, chitosan still has degradation and swelling limitations. Hence, chitosan hydrogel blends were incorporated with cellulose particles and were prepared as ink material. The hydrogels were successfully synthesized via thermo-responsive sol-gel method. Fourier transform infrared spectroscopy (FT-IR) analysis showed that the gelation of hydrogels formed a semi-interpenetrating network of ionically crosslinked chitosan and cellulose particles. Rheological tests have shown that the hydrogels exhibited shear thinning property necessary for printing. However, high cellulose amounts caused clogging during printing, and the presence of water limited the structural rigidity of the printed product. Besides this, it was found that the addition of cellulose was able to increase swelling, decrease degradation rate, and decrease gelation time, but the effect is not significant for any of these three properties.

Keywords: Additive manufacturing, Biomaterial, Thermoresponsive gelation, Tissue engineering, Cartilage engineering

1.0 INTRODUCTION

Fabrication via three-dimensional (3D) printing is becoming prominent nowadays, both in industry and in research. Before, it was mostly used for constructing prototypes, but now it is also utilized in manufacturing end-products. Recent developments on 3D printing technology includes reduction in cost and improvement of printing parameters such as print precision, resolution, and speed. These developments allowed the construction of complex and cost-efficient 3D structures, which leads to the emergence of 3D printing in biomedical and tissue engineering applications. Examples of 3D printed biomedical materials are anatomic models, drug delivery systems, permanent implants, prothesis, and biodegradable tissue scaffolds [1,2].

Among the mentioned products, biodegradable tissue scaffolds made from biomaterials are of great interest in regenerative treatment of tissue and organ defects. Scaffolds for bone, cartilage, blood vessels, and nerve tissues are being developed globally. The scaffold works by implanting and integrating it into the defect area. It acts as a mechanically supportive template for tissue regeneration. It aids cell attachment, migration, and proliferation. Once the newly healed tissues are formed, the scaffold will resorb or degrade [3]. Compared with other methods like autografts and allografts, tissue engineering is not constrained by donor tissue shortage and donor-site morbidity. The success of tissue regeneration highly depends on scaffold properties. Scaffolds must be able to replicate the functional properties of the surrounding extracellular matrix of the target tissue. Ideally, the scaffolds, must be biocompatible,

biodegradable, porous, and it must have mechanical properties similar with the target tissue [4,5].

Fabrication of biomaterial scaffolds can benefit significantly from 3D printing since employing this technique allows relatively easier and more accurate production of complex structures similar to that of human tissues. Additionally, the scaffolds can be made patient-specific, making sure that there will be no problems regarding possible implant-host mismatch [1]. 3D printing of tissue scaffolds has two important components: the 3D printer and the biocompatible ink material. As mentioned, recent advancements made 3D printers with excellent printing quality accessible. However, selection of proper printable ink materials remains to be an obstacle.

Hydrogels, defined as highly hydrated three-dimensional networks of polymer, are considered as the ideal ink material for scaffolds. It can mimic the extracellular environment of native tissues, and it can be easily functionalized to control its properties [6,7]. Most hydrogels are made from synthetic polymers such as polyethylene glycol, polyacrylamide, and poly(vinyl alcohol). Although these synthetic polymers have tunable properties, its biocompatibility is far from ideal [8]. The use of natural hydrogels is suggested as an alternative because of its better biological properties than synthetic ones. Most can be naturally sourced and can be inexpensive [6]. However, there are limited progress and development in natural hydrogels as biological ink material.

Chitosan, in its hydrogel form, is highly recommended to be used as ink material. Chitosan is an abundant polysaccharide biopolymer derived from the alkaline deacetylation of chitin. It is polycationic, non-toxic, and biodegradable [9,10]. Most importantly, the hydrogel form of chitosan has the rheology necessary for 3D printing [11]. Aside from these properties, the structure of chitosan is similar with those of gylcosaminoglycans, which are important structural components of the extracellular matrix. It was also found that it can enhance adhesion, proliferation, and functionality of various cell types [9]. However, its swelling and degradation properties are still limited. To address this, compatible cellulose particles are proposed to be incorporated into the chitosan structure. Cellulose, like chitosan, is a biocompatible and biodegradable polymer. It is a widely used additive because it has excellent binding and interactions with other polymers [12]. Furthermore, cellulose particles are ideal to be paired with chitosan because the structure of these two polymers are very similar, which makes the two polymers compatible [13].

This study aims to prepare a natural hydrogel blend composed of chitosan matrix and cellulose particles as potential extrusion 3D printer bioink material. The hydrogel is obtained from mixing cellulose particles, chitosan solution, and β-gylcerophosphate (β-GP), a non-toxic gelation agent. Specifically, it intends to determine the effect of addition of cellulose on swelling and degradation properties, and to investigate the rheological characteristics of the resulting hydrogel for printability assessment. The rheology is assessed based on the requirement for extrusion-based 3D printers. The study focused only on characterizing the composition, swelling, in-vitro degradation, and rheological properties of the hydrogel. No biological tests were employed in this study.

2.0 METHODOLOGY

Materials

All chemicals are analytical-grade reagents and used as-received without any further purification. The following reagents were used as starting material for the hydrogels: microcrystalline cellulose powder with particle size of 50 µm, chitosan powders (MW = 1,250,000; υ = 587.9 cps; DA = 93.09%), and β-gylcerol phosphate disodium salt pentahydrate. All materials were purchased from Glentham Life Sciences Ltd..

Preparation of Cellulose Suspension

The initial microcrystalline cellulose particles were subjected to hydrochloric acid (HCl) hydrolysis under hydrothermal conditions to decrease its particle size. The methodology used is based on the work of Yu et al., which was able to facilely produce high yields of stable cellulose nanocrystals via simple hydrothermal conditions [14]. The initial cellulose powders were dissolved and dispersed in 6.0 M HCl. The resulting solution was placed in a makeshift vessel made from an autoclave bottle covered with layers of aluminum foil. The vessel was heated in an oven at varying temperatures and reaction times. The resulting suspension was cooled down and was centrifuged at 4500 rpm for 15 minutes. Then, it was washed and diluted with cold distilled water several times to remove the residual acid. Once it reached a neutral pH, the suspension was stored. The final particle size and distribution of resulting cellulose was measured using dynamic light scattering particle analyzer following ASTM E3247-20 and with distilled water as solvent. The parameters that resulted with the smallest particle size were used for the whole study.

Synthesis and Gelation Of Hydrogels

The chitosan hydrogel samples were formed via a thermally induced sol-gel reaction using β-GP as gelation agent. The chitosan powders were first dissolved in an acetic acid solution. Crosslinking was done by slowly adding the β-GP while the polymer solution was immersed in an ice bath at 5 ^{o}C. The solution was mixed continuously until the β-GP was completely dissolved. Gelation was initiated by placing the resulting solution in a preheated oven at 45 ^{o}C. The samples were removed once it gelled completely. The cellulose reinforced hydrogels were synthesized similarly, but with the addition of varying amounts (0, 0.5, 0.75, and 1 wt%) of homogenized cellulose suspension. The suspension was added to the chitosan solution before the addition of β-GP and initiation of gelation. A flowchart of the synthesis of cellulose – chitosan hydrogel was provided in Figure 1.

Gelation was investigated by means of inverted vial test. For every set time interval, the vial containing the hydrogel was taken out of the oven and was inverted to check if it has fully gelled. The time when the samples does not flow anymore was taken as the gelation time. Thermoreversibility of the hydrogels were also examined by storing the hydrogels in a cold-water bath maintained at temperatures below 5 ^{o}C for 24 hours.

Hydrogel Characterizations

Compositional analysis

The precursor materials and all hydrogel settings underwent FT-IR analysis to determine any changes in functional groups during gelation.

Swelling and in-vitro degradation tests

The samples were first dried in a desiccator overnight, and the dry mass ($m_{initial}$) were recorded. For the swelling experiments, the samples were immersed in 15 ml phosphate-buffered saline (PBS) solution incubated at 37 °C for predetermined time intervals. Upon reaching the set time, the samples were carefully removed and were dried using filter paper. It was immediately weighed, and the swollen mass of the hydrogel ($m_{swollen}$) was recorded. The swelling ratio was calculated using the following equation:

$$\text{swelling ratio} = \frac{m_{swollen} - m_{initial}}{m_{initial}} \quad (1)$$

The in-vitro degradation properties were characterized by immersing the hydrogels in hydrolytic and enzymatic settings. For the hydrolytic setting, PBS solution was used as immersion medium. PBS solution with additional lysozyme (1.5 µg/ml) as enzyme catalyst was used for enzymatic setting. The hydrogel samples were immersed in the described solutions and were placed in an incubator at 37 °C. After predefined time intervals, the samples were taken out and washed with distilled water. The samples were dried in a desiccator overnight, and the samples were weighed after (m_{time}). The %mass loss was calculated using the following equation,

$$\%\text{mass loss} = \frac{m_{initial} - m_{time}}{m_{initial}} \times 100\% \quad (2)$$

Preliminary Printability Assessment And Rheological Measurements

Preliminary assessment of printability was done by manually simulating the printing process using flat tip syringes. The hydrogels were injected onto a flat glass surface layer by layer. Injecting through a flat tip syringe is similar to extrusion-based 3D printer set-up wherein a cartridge pump applies pressure to a syringe-like container connected to the nozzle. This simple experiment determined whether the hydrogels can easily flow when pressure is applied and check if clogging occurs. Injectability and continuity of resulting layers were observed. Injectability is examined by checking if the hydrogel successfully flows out of the syringe to form layers and without causing any clogs. Continuity is evaluated by observing whether there are gaps or spaces within the formed layers and if the layers are stable for a long time. When both these criteria were observed, then the result is positive.

To further understand the printability of the hydrogels, samples with positive and consistent results from the simulation were subjected to rheological measurements using a cone and plate rheometer. The following rheological tests were performed: flow sweep, oscillation amplitude sweep, and oscillation frequency sweep. All rheometer measurements were conducted under room temperature.

In flow sweep measurement, a plot of instantaneous viscosity as a function shear rate was obtained. The shear viscosity of the samples was measured along shear rates of 0.01 – 1000 s^{-1}. Then, oscillation amplitude sweep test was conducted at a constant frequency of 1 Hz to define the linear viscoelastic region (LVE). This measures the viscosity and shear moduli as a function of oscillation strain. Information obtained from this plot was used to establish the strain amplitude for the oscillation frequency sweep test. Finally, the frequency sweep test was done at 0.01 – 100 Hz using the constant strain rate from the LVE. This test describes the viscoelastic behavior of the hydrogel. A plot of storage modulus (G') and loss modulus (G") versus frequency was obtained.

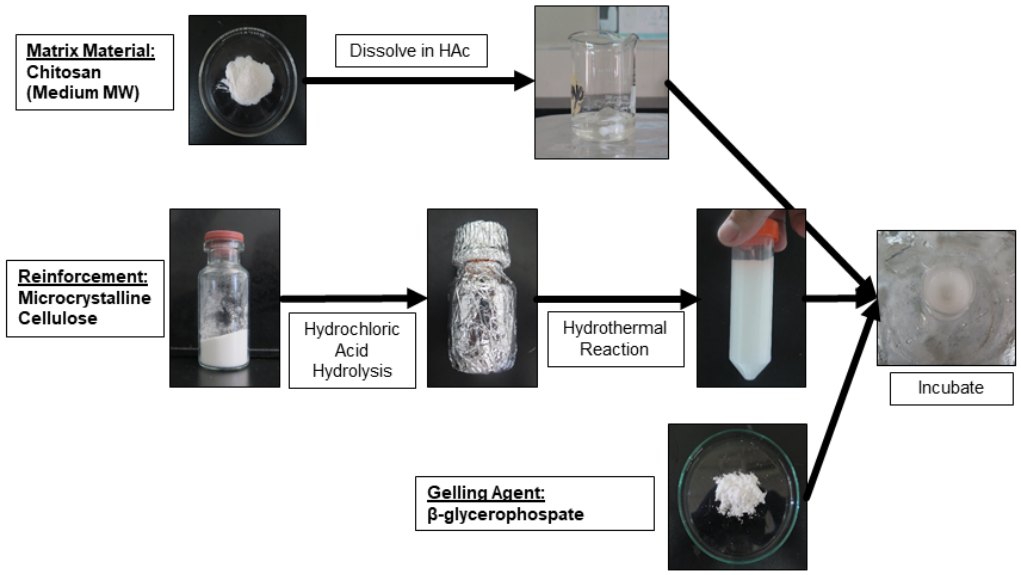

Figure 1. Experimental flowchart for synthesis of cellulose – chitosan hydrogel

Test printing of hydrogels

After choosing a suitable cellulose – chitosan hydrogel composition, the synthesized sample was tested for printing using the paste extruder system at room temperature. The 3D printer model is Ultimaker 2+ with Discovery paste extruder attached to it. It is a commercially available 3D printer and is inexpensive compared to other models. It is a direct extrusion type 3D printer, and it has a geared feeder that applies pressure for the ink material to flow. Before loading, the hydrogels, which were stored in refrigerator, were first allowed to equilibrate to room temperature and was placed in a desiccator to remove any excess water. Then, it was loaded into the syringe-like container. Printing was tested by setting the flow rate greater than 400%. The continuity and stability of layers formed were evaluated.

3.0 RESULTS AND DISCUSSION

Physico-Chemical Properties Of Hydrogels

Initially, nano-level cellulose particles were targeted after the hydrolysis. However, the methodology has a risk of carbonization [14]. If the resulting cellulose suspension has a light brown to black color, then the cellulose has carbonized and cannot be used. Different temperatures and hydrolysis times were tested to determine the parameters that would give the smallest particle size with no signs of carbonization. After several trials, it was established that at 85 ^{o}C for 2 hours the resulting suspension does not undergo carbonization, and it resulted to the smallest particle size. The smallest measured mean particle size is 1409.5 ± 236.8 nm. The particle decreased to about 97.18% of its initial size, however, it did not attain the target of nano-level particles. This setting was employed in the cellulose suspension preparation.

The FT-IR spectra of the initial microcrystalline cellulose, hydrolyzed cellulose, and carbonized cellulose (Figure 2) gave a better understanding of the hydrolysis process. Peaks shown in Figure 2.a.i. were all associated with cellulose. Peaks at 3332, 2897, 1427, and 1315 cm^{-1} correspond to OH, CH, CH_2, CH bending, respectively. Peaks assigned to C-O-C bonds were found at 1161, 1103, and 1052 cm^{-1}, while the 893 cm^{-1} peak is attributed to β-glycosidic linkage [15]. Due to the presence of sharp bands in 1427 and 1315 cm^{-1} and the absence of out-of-bending OH peak, the precursor microcrystalline cellulose exhibits a cellulose Iβ structure. Ideally, the type of structure of cellulose before and after hydrolysis should be the same. Based on Figure 2a.ii., characteristics pertaining to cellulose Iβ were exhibited by hydrolyzed cellulose, showing evidence that the hydrolysis did not cause any chemical changes. All peaks of precursor cellulose were similar with hydrolyzed cellulose except for 1635 cm^{-1} peak in hydrolyzed cellulose. This peak pertains to the OH adsorbed during hydrolysis. For carbonized samples, peaks for cellulose Iβ structure were not present (area encircled in Figure 2a.iii.). This indicates that a chemical change like carbonization happened during hydrolysis [14].

The FT-IR spectra of chitosan, β-GP and chitosan hydrogel were shown in Figure 2b. In Figure 2b.i., all peaks were characteristic of chitosan. The important peaks are the broad peaks in the 3350 and 3294 cm^{-1} region associated with both OH and NH bands, 2868 cm^{-1} for aliphatic CH, 649 cm^{-1} for C=O and amide I, 1585 cm^{-1} for amide II, 1375 cm^{-1} for CH_2OH, 1069 and 1026 cm^{-1} for CO stretching of CH_2 and CH_2OH, and lastly 893 cm^{-1} for C-O-C [16]. In Figure 2b.ii., the identifying peaks for β-GP were 3209 cm^{-1} for OH and the phosphorus groups in the 500 – 1100 cm^{-1} range [17]. The peak in 1668 cm^{-1} represents the hydration peak of β-GP [18]. In the hydrogel spectrum (Figure 2b.iii.), no new additional peaks are formed, and all peaks are present either in chitosan or in β-GP spectra. This indicates that no chemical reaction occurred during gelation, and the interactions in the resulting hydrogel are physical interactions. Moreover, the OH and NH shifted to lower wavenumbers in the hydrogel spectrum. This implies that hydrogen bonding exists between chitosan chains and chitosan and β-GP. It was also observed that the NH peak becomes blunt and the number of peaks pertaining to phosphorus groups decreased, both showing evidence of a protonated amino group. The protonated amino group has a positive charge and likely interacts with the negative phosphate groups of β-GP by forming ionic crosslinking. Aside from the ionic crosslinking and hydrogen bonding, there also exists a hydrophobic interaction between two chitosan chains. This hydrophobic interaction contributes to the charge density of the hydrogel [19–21].

Figure 3a compares the spectra of all cellulose-chitosan hydrogel settings. All settings have similar major peaks, and no new peaks were observed. This means that interaction between chitosan and cellulose is purely physical in nature. It is proposed that hydrogen bonds exist between OH groups in cellulose and OH and NH_2 groups in chitosan [22].

From the FT-IR analysis, it was proposed that the composite hydrogel is comprised of semi-interpenetrating network of ionically crosslinked chitosan and cellulose particles with chains physically entangled with each other. The cellulose particles diffused into the chitosan network, and interact via hydrogen bonding [13]. Figure 3b illustrates the semi-interpenetrating network and it includes the different interactions present, namely, ionic crosslinking between β-GP and chitosan, hydrogen bonding between chitosan chains, chitosan-cellulose chains, and chitosan-β-GP, and lastly, hydrophobic interactions between chitosan chains [23].

The thermoreversibility of gelation was also investigated. After 24 hours of cold storage, it was found that the gels did not turn back into its initial sol state, showing irreversibility. This implies that a strong hydrogen bonding was involved in its molecular structure, and it is likely to be the dominant interaction. Hydrogen bonds are known to be independent to temperature [24].

Effect of cellulose addition on chitosan hydrogel properties

Based on the inverted vial test, the gelation time for the pure chitosan hydrogel was measured to be 45 minutes. For 0.5 wt%, 0.75 wt%, 1 wt%, gelation times were 40 minutes, 35 minutes, and 20 minutes, respectively. It was observed that when the cellulose content was increased, the gelation time decreased. The addition of cellulose makes the gelation of the hydrogel faster. This can be explained by the increase of intermolecular interactions and entanglements in the system due to presence of cellulose. The more entangled polymer chains present in a hydrogel, the faster the gelation [25].

The results of the hydrolytic degradation experiments were shown in Figure 4a. This accounts the mass loss due to scission of chains caused by reaction with ion-containing water. It was

noticed that there is a significant mass loss after the first day of immersion. Observed mass loss values for the hydrogels reached as high as 89%. After the 21-day period, there is still a small amount of hydrogel left and it does not dissolve completely, but it loses a significant percentage of its mass. The high initial mass loss is inferred to be caused by presence of ether and polar groups in chitosan. These functional groups make the hydrogels susceptible to water [26]. Comparing the hydrogel settings, the 1 wt% has the lowest mass loss value. The addition of cellulose lowered the degradation rate of the hydrogel, but the decrease is not significant.

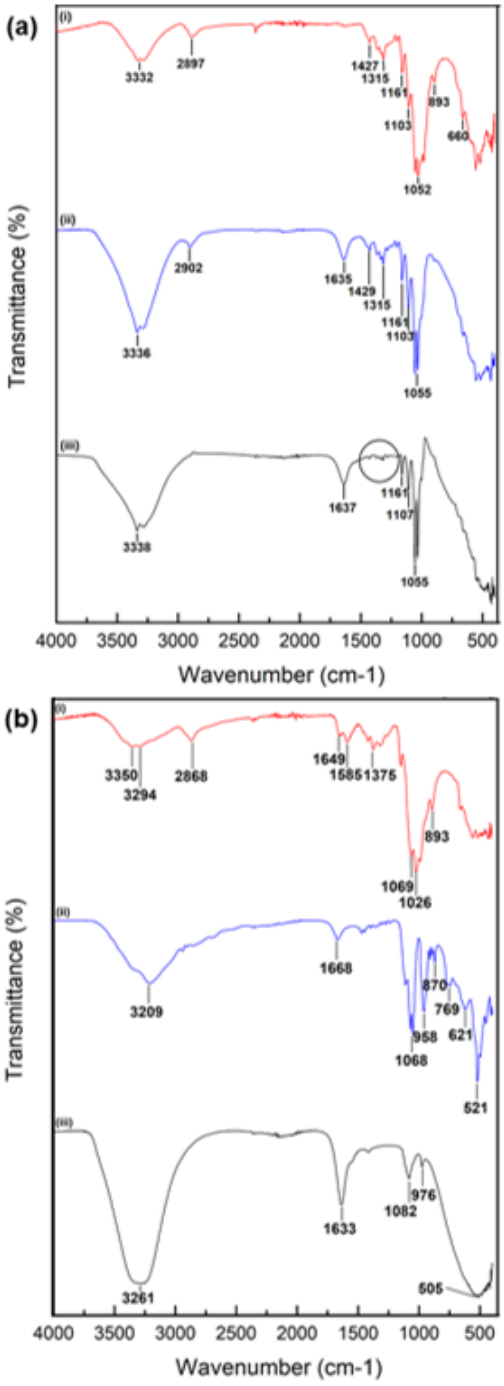

Figure 2. a) FT-IR spectra of (i) microcrystalline cellulose, (ii) hydrolyzed cellulose, (iii) carbonized cellulose. b) FT-IR spectra of (i) chitosan powder, (ii) β-GP, (iii) chitosan hydrogel

The trend and behavior observed in the enzymatic degradation is similar with what was obtained in hydrolytic degradation tests, as shown in Figure 4b. There is a high value of degradation for the first day of immersion, and after 21 days the hydrogel did not dissolve but lost a big percentage of its mass. Also, 1 wt% setting has the lowest mass loss value, and the mass value decreased with increasing cellulose amount. This indicates that the addition of lysozyme does not significantly catalyzed degradation, and it was water that mainly cause degradation. The addition of cellulose, although it decreased the degradation rate of the hydrogel, is not significant enough.

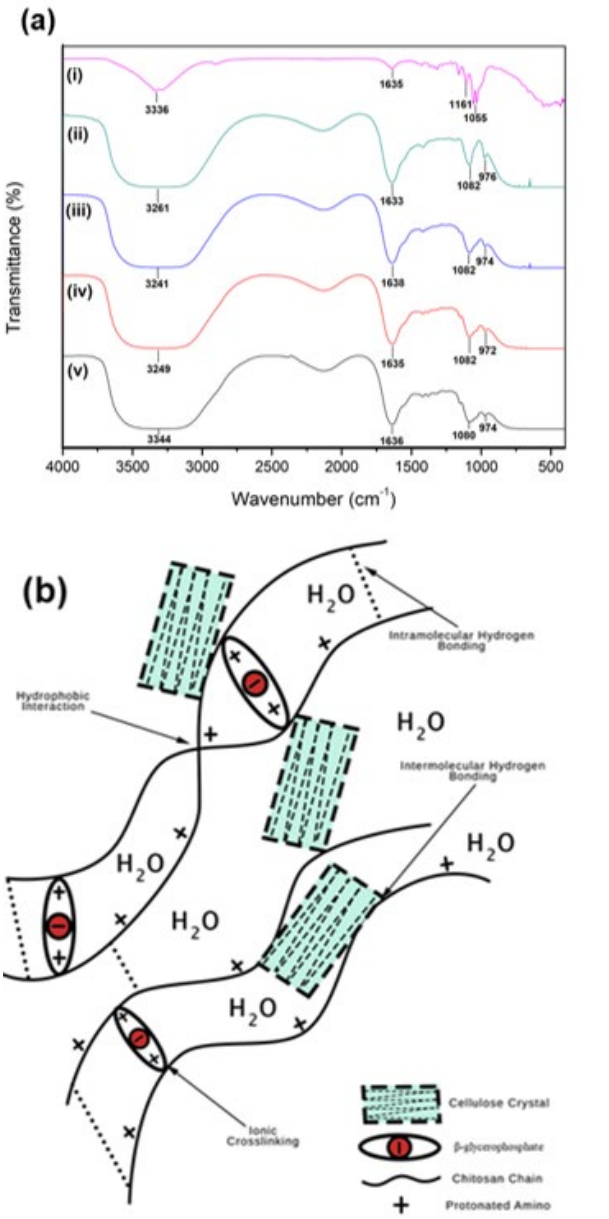

Figure 3. a) FT-IR spectra of (i) hydrolyzed cellulose, (ii) chitosan hydrogel, (iii) 0.5 wt%, (iv) 0.75 wt%, (v) 1 wt% cellulose – chitosan hydrogel. b) Illustration of interactions present on polymer chains in the composite hydrogel

The differences between mass loss values of each setting are small. The degradation is too rapid for the intended application. Thus, there is a need to slower the degradation rate in a way that it will be tuned with the regeneration of tissues. The slight decrease in degradation might have been caused by the greater molecular interactions caused by cellulose addition. The additional hydrogen bonding provided by cellulose might have strengthened the interactions in between bonds, making bond breaking slightly difficult. Although the cellulose decreased the mass loss values in both hydrolytic and enzymatic set-ups, its effect is not significant.

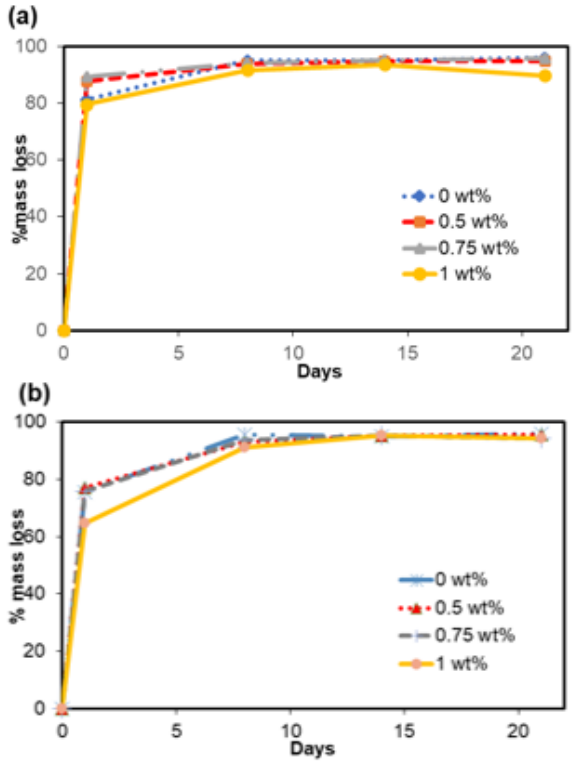

Figure 4. a) Plot of hydrolytic degradation (%mass loss vs days) for 21 days. b) Plot of enzymatic degradation (%mass loss vs days) over period for 21 days.

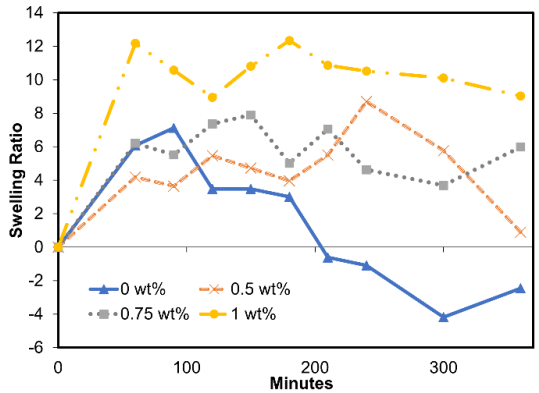

Figure 5. Plot of swelling experiments in PBS immersion for 6 hours.

The swelling behaviors of the hydrogels over a period of 6 hours were shown in Figure 5. The observed swelling capacity of the chitosan hydrogels were around 2 – 14%. Moreover, the swelling ratio does not equilibrate or reach a constant value. After 180 minutes, the swelling ratio starts to decrease. The pure chitosan hydrogels even obtained negative values. This noticeable decrease is associated with the fast degradation occurring in the hydrogels. It is possible that the increase in swelling was being countered by degradation wherein the rate of bond cleavage occurs faster than the rate of water diffusion. Given this, it was speculated that the degradation of the hydrogels occurs via surface erosion [26]. Comparing the obtained values for each hydrogel settings, the 1 wt% setting gives off the highest swelling ratio values. However, the differences are not significant enough to say that the cellulose can increase the swelling ratio.

Effect of cellulose addition on chitosan hydrogel properties

Printability was first assessed by testing injectability using flat tip syringes. During injection, there was a significant presence of water in settings containing cellulose. The water was from the solvent of the cellulose suspension, and it could have diffused inside the polymer network during gelation even after drying. A gel layer will be injected, then there will be a splash of water after. This pattern influenced the injection of layers, and it made the layer discontinuous. In terms of print characteristics, the most consistent in producing layers with enough structural rigidity was the 0.5 wt% setting. The 0 wt% and 0.25wt%, although both produced continuous layer, the layers were not rigid. Higher cellulose amounts exhibited clogging of the syringe and pushing becomes more difficult. It was initially speculated that this behavior was due to the high viscosities resulting from high particle content. This is based from the Krieger-Dougherty relationship wherein the presence of higher volume fraction of solid particles in a suspension results to greater viscosity values [27]. To further verify and expound on this hypothesis, the samples, specifically pure chitosan and the 0.5wt% setting, were subjected to rheological tests. Only the 0.5 wt% was chosen because it is the only setting that did not cause clogging and can form stable layers, making it ideal for application compared to other settings.

The LVE was first determined from oscillation amplitude sweep of the 0.5 wt% setting as shown in Figure 6a. Based on the plot, the 10% strain was a safe strain level for both samples because the G' and G" curves are horizontal at that point. At low strain levels, the G', which describes elastic behavior, was greater than G", which is associated with viscous properties. This shows that the hydrogel was more gel-like than liquid in low strain levels. This behavior is helpful in holding the ink, which should not flow out when it is in static state inside the nozzle of the printer. At high strain levels, the G" was greater than G', this means that the hydrogel is liquid-like and will flow at high strains. This is helpful in extruding the hydrogel, since applying strain or pressure will make the hydrogel flow. To better investigate this characteristic, the samples underwent flow sweep.

Figure 6b shows the flow sweep plots for 0 wt% and 0.5 wt% cellulose samples. The measured viscosities for both settings were still within the workable material viscosity range for an extrusion type printer (0.03 – 60,000 Pa•s) [28]. Furthermore, it was observed that the presence of cellulose slightly decreased the viscosity of chitosan hydrogel. This is not in agreement with what was expected and what was observed during simulation. The difference in results may have been caused by the

presence of water in the hydrogel that could have affected the rheometer measurements. Even with the increase in intermolecular interactions, the significant presence of water decreased the viscosity. This makes the hydrogel more susceptible to shear. There are studies that showed water content in hydrogels could decrease the strength, therefore, water in the samples could be the main contributor of this observed behavior [29,30]. In addition, it is possible that the clogging in the initial simulations may have not been caused by high viscosity, but rather the cellulose particles accumulating in the syringe needle. Since higher cellulose means greater number of particles, there will be more particles that can accumulate in the needle. It is recommended that the cellulose used must not be in suspension form. This will reduce the effect of water in the rheological measurements.

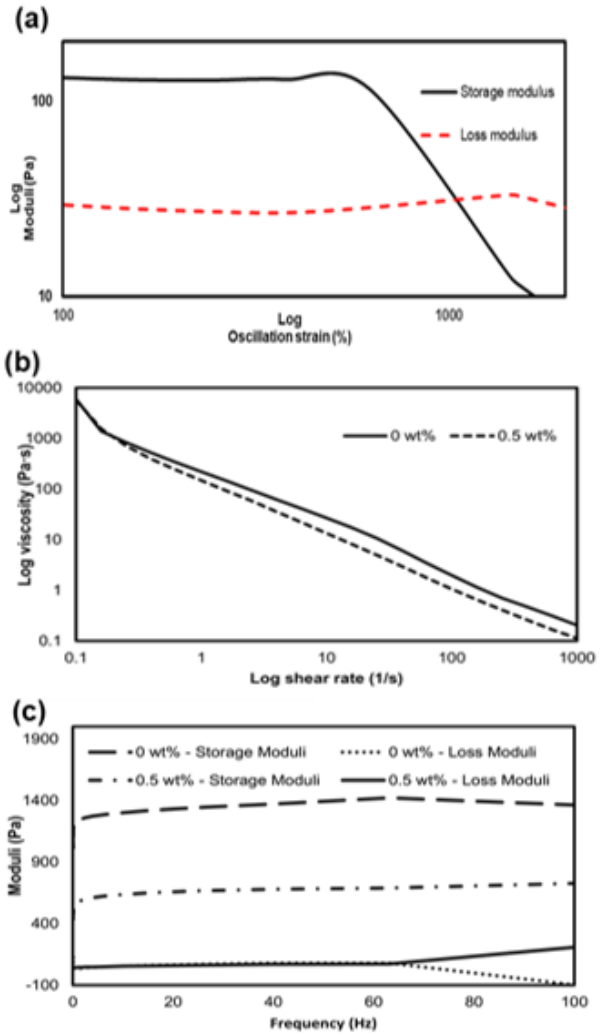

Figure 6. a) Plot of storage modulus (G') and loss modulus (G") vs strain of 0.5 wt% setting (b) Log plot of viscosity vs shear rate for 0 wt% and 0.5 wt% settings, (c) Plot of moduli vs frequency of 0 wt% and 0.5 wt% settings.

The flow sweep results were fitted with the Power Law equation to check if the hydrogels manifest a well-defined shear thinning response. Power Law equation has the form shown in Eqn. (3):

$$\eta = K\gamma^{n-1} \quad (3)$$

where η is the measured viscosity, γ is the shear rate, and both K and n are the shear thinning coefficients [31].

The obtained R^2 were 0.9947 and 0.9943 for 0 wt% and 0.5 wt% respectively. Since the R^2 are near 1, then the viscosity of both settings follows the Power Law. Using the Power Law equation, the shear thinning coefficient n were calculated. It can be used as a metric to identify shear thinning. The n values obtained were 0.0425 and 0.1042 for 0 wt% and 0.5 wt% respectively. Both coefficients are below 0.20, thus, the hydrogels exhibit shear thinning and are pseudoplastic in nature.

Lastly, the plots of shear moduli against varying frequencies (Figure 6c) were obtained from the oscillation frequency sweep. For both settings, G' > G" in large magnitudes. This denotes that both hydrogels exhibit viscoelastic solid-like behavior rather than fluid-like. This behavior is helpful in 3D printing because it shows that the hydrogel could produce solid constructs with good dimensional stability and structural fidelity during and after printing. Also, the G' and G" curves were almost parallel with each other. This indicates that the hydrogel contains a closely crosslinked structure [32].

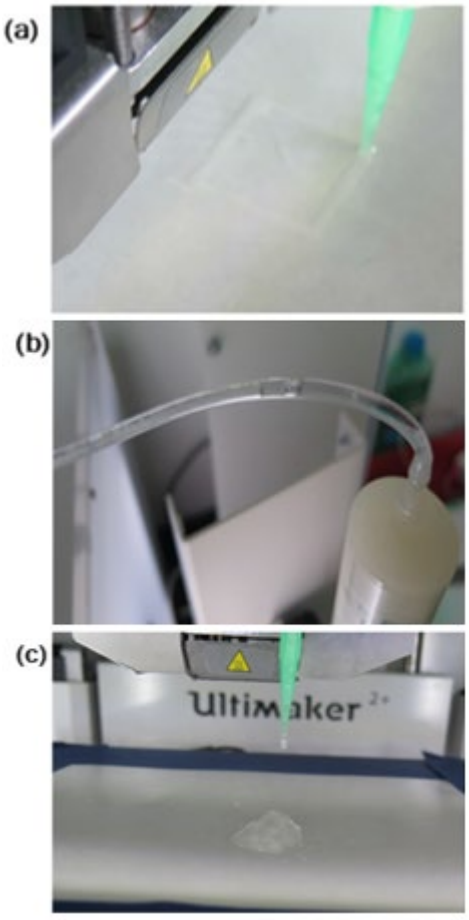

Figure 7. Figure 7. (b) Image of water present in connecting tubes of 3D printer (c) Image of extruded layers of 0.5 wt% cellulose – chitosan hydrogel that collapsed entirely.

The G' is of great interest in describing the strength of hydrogels. A higher G' can be associated with higher shear mechanical properties. The G" for both settings were similar, but for the G' there is a difference. The G' for 0 wt% is always greater than 0.5 wt% in all frequencies. This signifies that the

addition of cellulose lowered the strength of the hydrogel instead of increasing it. This contradicts the expected results but agrees with the flow sweep results. Similar with what was mentioned earlier, the deviation may have been caused by the presence of water. This could have lowered the viscosity and shear property. Drying only removed the surface water but was not able to remove water that diffused in the inner networks of the hydrogel. This affects the elastic properties and have weakened the interactions inside the hydrogel. It is recommended for the samples to undergo further mechanical tests via compression.

The 0.5 wt% setting was tested for actual 3D printing test. In the trial, the 0.5 wt% hydrogel was successfully extruded out of the nozzle with material flow rate of around 400% - 700% as presented in Figure 7a. The force needed to push the hydrogels was still below the maximum 1000 psi for the paste extruder. The extrusion resulted to layers of cellulose – chitosan hydrogel; however, these layers were not continuous due to the presence of water piling up in between the layers. Even after drying, water was present in connecting tubes of the printer (shown in Figure 7b) and it disrupts the continuity of layers. Due to this, it was difficult to form a stable 3D construct. Only a few layers could be formed because large constructs will contain significant amounts of water. Significant amounts of water lessen the rigidity of the construct causing it to collapse like in Figure 7c. It was suggested that further optimization of the printing process should be studied.

4.0 CONCLUSION

The study was able to synthesize a hydrogel blend containing an ionically crosslinked chitosan and cellulose particles via a thermally induced sol-gel transition method. Based on FT-IR data, the synthesized hydrogel is made up of semi-interpenetrating networks of chitosan and cellulose particles. The molecular interactions in the hydrogel are all physical in nature. The added cellulose interacts with chitosan via strong hydrogen bonding. The addition of cellulose improved swelling behavior and decreased the gelation time and the degradation rate of the chitosan hydrogels; however, the improvement is not significant enough. The rheology of the hydrogels was examined, and it was determined that the 0.5wt% cellulose has the potential to be printable. It exhibits shear thinning property and it has an elastic solid-like behavior for rigidity. However, the addition of cellulose showed a decrease in G', which is indicative of a decrease in shear properties and viscosity. This decrease is attributed to the significant presence of water in the hydrogels.

A quick printing was done, but there is still a need for more improvement and optimization. One is the removal of significant amount of water in the hydrogels, which makes the printing inconsistent and difficult. Suspension forms of cellulose are not recommended to be used. Lastly, biological characterizations of the hydrogels are now being evaluated as next step of research.

Acknowledgement

Financial support was given by the Department of Science and Technology - Philippine Council for Industry, Energy and Emerging Technology Research and Development through the Young Innovators Program. J.K.C. also extends his thanks to the Crisostomo A. Ortigas Professorial Chair awarded through the Engineering Research and Development Foundation, Inc.

References

[1] Yan Q., Dong H., Su J., Han J., Song B., Wei Q., and Shi Y. 2018. A Review of 3D Printing Technology for Medical Applications. *Engineering*, 4: 729–742. https://doi.org/10.1016/j.eng.2018.07.021.

[2] Mishra S. 2016. Application of 3D printing in medicine *Indian Heart Journal*, 68: 108–109. https://doi.org/10.1016/j.ihj.2016.01.009.

[3] Chung S. and King M.W. 2011. Design concepts and strategies for tissue engineering scaffolds. *Biotechnology and Applied Biochemistry*, 58: 423–438. https://doi.org/10.1002/bab.60.

[4] Vinatier C. and Guicheux J. 2016. Cartilage tissue engineering: From biomaterials and stem cells to osteoarthritis treatments. *Annals of Physical and Rehabilitation Medicine*, 59: 139–144. https://doi.org/10.1016/j.rehab.2016.03.002.

[5] O'Brien F.J. 2011. Biomaterials & scaffolds for tissue engineering. *Materials Today*, 14: 88–95. https://doi.org/10.1016/S1369-7021(11)70058-X.

[6] Bishop E.S., Mostafa S., Paksava, M., Luu H.H., Lee M.J., Wolf J.M., Ameer G.A., He T.C., and Reid R.R. 2017. 3-D bioprinting technologies in tissue engineering and regenerative medicine: Current and future trends. *Genes and Diseases*, 4: 185–195. https://doi.org/10.1016/j.gendis.2017.10.002.

[7] Chimene D., Lennox K., Kaunas R., and Gaharwar A. 2016. Advanced Bioinks for 3D Printing: A Materials Science Perspective. *Annals of Biomedical Engineering*, 44: 2090–2102. https://doi.org/10.1007/s10439-016-1638-y.

[8] Teßmar J., Brandl F., and Göpferich A. 2009. Hydrogels for tissue engineering. *Fundamentals of Tissue Engineering and Regenerative Medicine,* 101: 495–517. https://doi.org/10.1007/978-3-540-77755-7_37.

[9] Ahsan S., Thomas M., Reddy K., Sooraparaju S., Asthana A., and Bhatnagar I. 2018. Chitosan as biomaterial in drug delivery and tissue engineering. *International Journal of Biological Macromolecules*, 110: 97–109. https://doi.org/10.1016/j.ijbiomac.2017.08.140.

[10] Boonruam P. and Wattanachai P. 2021. Effects of chemical compositions of chitosan-based hydrogel on properties and collagen release. *ASEAN Engineering Journal*, 11: 85–100. https://doi.org/10.11113/AEJ.V11.16684.

[11] Rahimnejad M., Labonté-Dupuis T., Demarquette N., and Lerouge S. 2020. A rheological approach to assess the printability of thermosensitive chitosan-based biomaterial inks. *Biomedical Materials*, 16. https://doi.org/10.1088/1748-605X/abb2d8.

[12] De France K., Hoare T., and Cranston E. 2017. Review of Hydrogels and Aerogels Containing Nanocellulose. *Chemistry of Materials*, 29: 4609–4631. https://doi.org/10.1021/acs.chemmater.7b00531.

[13] Sampath U., Ching Y., Chuah C.,Singh R., and Lin P. 2017. Preparation and characterization of nanocellulose reinforced semi-interpenetrating polymer network of chitosan hydrogel. *Cellulose*, 24: 2215–2228. https://doi.org/10.1007/s10570-017-1251-8.

[14] Yu H., Qin Z., Liang B., Liu N., Zhou, Z., and Chen L. 2013. Facile extraction of thermally stable cellulose nanocrystals with a high yield of 93% through hydrochloric acid hydrolysis under hydrothermal conditions. *Journal of Materials Chemistry A*, 1: 3938–3944. https://doi.org/10.1039/c3ta01150j.

[15] Pachuau L., Dutta R., Hauzel L., Devi T., and Deka D. 2019. Evaluation of novel microcrystalline cellulose from Ensete glaucum (Roxb.) Cheesman biomass as sustainable drug delivery biomaterial. *Carbohydrate Polymers*, 206: 336–343. https://doi.org/10.1016/j.carbpol.2018.11.013.

[16] Assaad E., Maire M., and Lerouge S. 2015. Injectable thermosensitive chitosan hydrogels with controlled gelation

kinetics and enhanced mechanical resistance. *Carbohydrate Polymers*, 130: 87–96. https://doi.org/10.1016/j.carbpol.2015.04.063.

[17] Skwarczynska A., Kaminska M., Owczarz P., Walkowiak B., Modrzejewska Z., and Bartoszek N. 2018. The structural (FTIR , XRD , and XPS) and biological studies of thermosensitive chitosan chloride gels with b -glycerophosphate disodium. *Journal of Applied Polymer Science,* 135 46459: 1–8. https://doi.org/10.1002/app.46459.

[18] Stuart B. 2004. Infrared Spectroscopy: Fundamentals and Applications, 1st ed., Wiley, New York.

[19] Deng A., Kang X., Zhang J., Yang Y., and Yang S. 2017. Enhanced gelation of chitosan / β -sodium glycerophosphate thermosensitive hydrogel with sodium bicarbonate and biocompatibility evaluated. *Materials Science and Engineering: C*, 78: 1147–1154. https://doi.org/10.1016/j.msec.2017.04.109.

[20] Kim S., Nishimoto S., Bumgardner J., Haggard W., Gaber M., and Yang Y. 2010. A chitosan / b -glycerophosphate thermo-sensitive gel for the delivery of ellagic acid for the treatment of brain cancer. *Biomaterials*, 31: 4157–4166. https://doi.org/10.1016/j.biomaterials.2010.01.139.

[21] Tang Y., Wang X., Li Y., Lei M., Du Y., Kennedy J., Knill C. 2010. Production and characterisation of novel injectable chitosan / methylcellulose / salt blend hydrogels with potential application as tissue engineering scaffolds. *Carbohydrate Polymers*, 82: 833–841. https://doi.org/10.1016/j.carbpol.2010.06.003.

[22] Meng G., Peng H., Wu J., Wang Y., Wang H., Liu Z., and Guo X. 2017. Fabrication of Superhydrophobic Cellulose / Chitosan Composite Aerogel for Oil / Water Separation. *Fibers and Polymers*, 18: 706–712. https://doi.org/10.1007/s12221-017-1099-4.

[23] Supper S., Anton N., Seidel N,, Riemenschnitter M., Curdy C., and Vandamme T. 2014. Thermosensitive chitosan / glycerophosphate-based hydrogel and its derivatives in pharmaceutical and biomedical applications. *Expert Opinion on Drug Delivery*, 11: 249–267. https://doi.org/10.1517/17425247.2014.867326.

[24] Tahrir F., Ganji F., Mani A., and Khodaverdi E. 2014. In vitro and in vivo evaluation of thermosensitive chitosan hydrogel for sustained release of insulin. *Drug Delivery*, 23 7544: 1–9. https://doi.org/10.3109/10717544.2014.932861.

[25] Ahmadi R., and De Bruijn J. 2008. Biocompatibility and gelation of chitosan-glycerol phosphate hydrogels. *Journal of Biomedical Materials Research Part A*, 86: 824–832. https://doi.org/10.1002/jbm.a.31676.

[26] Coury A. 2012. Chemical and Biochemical Degradation of Polymers Intended to be Biostable, in: B. Ratner, A. Hoffman, F. Schoen, J. Lemons (Eds.). *Biomaterials Science: An Introduction to Materials in Medicine*, 3rd ed., Academic Press, Oxford, 697–715.

[27] Choi G. and Krieger I. 1986. Rheological Studies on Sterically Stabilized Model Dispersions of Uniform Colloidal Spheres Volkingburg of the Dow Coming Corporate. *Journal of Colloid and Interface Science*, 113 101–113.

[28] Jungst T., Smolan W., Schacht K., Scheibel T., and Groll J. 2016. Strategies and Molecular Design Criteria for 3D Printable Hydrogels. *Chemical Reviews*, 116: 1496–1539. https://doi.org/10.1021/acs.chemrev.5b00303.

[29] Wei Q., Zhang Y., Wang Y., Chai W., Yang M., Zeng W., and Wang. 2015. Study of the effects of water content and temperature on polyacrylamide/polyvinyl alcohol interpenetrating network hydrogel performance by a molecular dynamics method. *e-Polymers*, 15: 301–309. https://doi.org/10.1515/epoly-2015-0087.

[30] Cui X., Zheng W., Zou W., Liu X., Yang H., Yan J., and Gao Y. 2019. Water-retaining, tough and self-healing hydrogels and their uses as fire-resistant materials. *Polymer Chemistry*, 10: 5151–5158. https://doi.org/10.1039/c9py01015g.

[31] Paxton N., Smolan W., Böck T., Melchels F., Groll J., and Jungst T. 2017. Proposal to assess printability of bioinks for extrusion-based bioprinting and evaluation of rheological properties governing bioprintability. *Biofabrication*, 9: https://doi.org/10.1088/1758-5090/aa8dd8.

[32] Huber D., Tegl G., Baumann M., Sommer E., Gorji E., Borth N., Schleining G., Nyanhongo G., and Guebitz G. 2017. Chitosan hydrogel formation using laccase activated phenolics as cross-linkers. *Carbohydrate Polymers*, 157: 814–822. https://doi.org/10.1016/j.carbpol.2016.10.012.